

Factors contributing to the onset of the Australian summer monsoon

By CHIH-WEN HUNG and MICHIO YANAI*

Department of Atmospheric Sciences, University of California, USA

(Received 27 September 2002; revised 12 August 2003)

SUMMARY

Using the reanalyses from the European Centre for Medium-Range Weather Forecasts, outgoing long-wave radiation (OLR) and precipitation data for 1979–93, this paper examines major factors contributing to the onset of the Australian summer monsoon. The low-level (850 hPa) westerly wind and convective activity (OLR, precipitation) over a region in northern Australia (NAU) are used to determine the onset dates. Composite results are then derived, based on these dates. Daily apparent heat source and apparent moisture sink values are obtained as residuals of the large-scale heat and moisture budgets to help clarify the roles of the various heating processes in the onset. Four major factors contributing to the onset are identified: (1) land–sea thermal contrast, (2) barotropic instability, (3) arrival of the Madden–Julian oscillation (MJO) and (4) intrusion of midlatitude troughs. The thermal contrast due to differential heating between land and sea acts as a seasonal preconditioning for the onset. The sensible heating over the continent leads to a reversal of meridional temperature gradient between the Australian continent and the Arafura Sea in a layer below 800 hPa in September–March, and sets up a thermally induced meridional–vertical circulation which helps to transport low-level moist air inland. The barotropic instability criterion is often met at 850 hPa in NAU several days prior to the onset. The sudden onset is then triggered by the arriving MJO and at times by the intrusion of a midlatitude trough.

KEYWORDS: Barotropic instability Heating processes over Australia Land–sea thermal contrast Madden–Julian oscillation

1. INTRODUCTION

It has been believed for many centuries that the land–sea thermal contrast is important for monsoons (e.g. Webster 1987; Webster *et al.* 1998), although some authors (e.g. Chao 2000; Chao and Chen 2001) challenged this view and argued that the existence of land is not a necessary condition for the presence of monsoons. Basically, landmass has two major effects on the large-scale atmospheric motion: (1) mechanical forcing due to topography and (2) thermal forcing due to land–sea contrast. To isolate clearly the role of the thermal effect, it is desirable to find a monsoon region without high land. The Australian summer monsoon seems an ideal candidate for examining the thermal effect in a pure form, because the flat land surface of Australia has no complex topography.

The Australian summer monsoon usually begins in December and ends in March. Its mature stage is characterized by heavy precipitation and low-level westerly wind over northern Australia and the Arafura Sea (McBride 1987; Manton and McBride 1992). This monsoonal nature of northern Australian climate (the seasonal precipitation and reversals of wind direction) was recognized in the early 20th century (Hunt *et al.* 1913). In the 1960s, several studies (e.g. Berson 1961) showed that the Australian summer monsoon has similarities to the Asian summer monsoon, such as its abrupt poleward shift, sudden onset over a large region and intraseasonal active–break periods.

There was little work on the Australian monsoon in the literature until the First Global Atmospheric Research Program Global Experiment (FGGE) in 1978–79 and the Australian Monsoon Experiment (AMEX) in 1986–87. The FGGE data made diagnostic analyses possible for the large-scale circulation associated with the Australian summer monsoon (e.g. Murakami and Sumi 1982a,b; Davidson *et al.* 1983). The AMEX

* Corresponding author: Department of Atmospheric Sciences, University of California, 405 Hilgard Avenue, Los Angeles, CA90095-1565, USA. e-mail: yanai@atmos.ucla.edu

observations, on the other hand, provided high-density synoptic and mesoscale data over northern Australia. The AMEX phase II fieldwork lasted 36 days from 10 January 1987, which was 4 days before the monsoon onset (Hendon *et al.* 1989). The success of the AMEX led to several detailed observational results, such as the vertical heating profiles in the northern Australian monsoon region (Frank and McBride 1989).

Besides these results from the special experiments, several authors made studies using longer records. Hendon and Liebmann (1990a,b) suggested that the Madden-Julian oscillation (MJO; Madden and Julian 1971, 1972) acts as a trigger for the monsoon onset, based on a composite study from station data obtained at Darwin in 1957–87. On the other hand, Davidson *et al.* (1983) studied the synoptic situations prior to the monsoon onset using operational analyses, and argued that midlatitude events play a role in the onset.

Despite these studies, the Australian summer monsoon has received relatively little attention compared to the Asian summer monsoon. Several gaps in our existing knowledge need to be addressed:

(1) The AMEX happened to be in an El Niño year. A late onset and large-scale sinking anomalies were observed in northern Australia. We feel that it is necessary to study large-scale atmospheric conditions for many years and use the composite method to describe more general situations.

(2) The composite studies from previous work were mainly from station data. The ‘reanalysis’ datasets are now available for study of 3-dimensional features of the Australian monsoon. The classic sea-breeze model associated with the land–sea thermal contrast can be re-examined. It is also possible to apply dynamic instability theories to the monsoon onset.

(3) In previous studies, the large-scale heat and moisture budgets have not been seriously examined in the Australian region. With the reanalysis datasets, heat and moisture budgets can be calculated for a more systematic examination of thermodynamic effects. For example, the role of sensible heating over the Australian continent can be studied.

(4) Previous observational works focus on different onset processes separately (e.g. MJO triggering, midlatitude events). It is desirable to present a unified view of the onset mechanisms and identify major factors contributing to the onset using composite results.

In this paper, we use the reanalysis dataset to calculate large-scale heat and moisture budgets, and the role of the land–sea thermal contrast in the Australian summer monsoon is re-examined. In section 2, the datasets, the definition of the onset and the composite method are described. In section 3, the composite features showing the heating profiles before/after the monsoon onset are presented. In section 4, four major factors contributing to the onset are discussed. Finally, section 5 presents conclusions.

2. DATA AND THE DEFINITION OF THE ONSET

(a) Data

The primary data used for this work is the 15-year (1979–93) European Centre for Medium-Range Weather Forecasts (ECMWF) reanalysis (ERA; Gibson *et al.* 1997). The daily outgoing long-wave radiation (OLR) measurements and monthly Climate Prediction Center Merged Analysis of Precipitation (Xie and Arkin 1997) for the same period are also used. In addition, large-scale heat and moisture budget residuals *apparent heat source*, Q_1 , and *apparent moisture sink*, Q_2 , (Yanai *et al.* 1973) are defined and

computed by:

$$Q_1 \equiv c_p \left(\frac{p}{p_0} \right)^\kappa \left(\frac{\partial \bar{\theta}}{\partial t} + \bar{\mathbf{v}} \cdot \nabla \bar{\theta} + \bar{\omega} \frac{\partial \bar{\theta}}{\partial p} \right) \quad (1)$$

and

$$Q_2 \equiv -L \left(\frac{\partial \bar{q}}{\partial t} + \bar{\mathbf{v}} \cdot \nabla \bar{q} + \bar{\omega} \frac{\partial \bar{q}}{\partial p} \right), \quad (2)$$

where θ is the potential temperature, q the mixing ratio, \mathbf{v} the horizontal velocity, ω the vertical p -velocity, L the latent heat of vaporization, $\kappa = R/c_p$ with R the gas constant, c_p the specific heat capacity of dry air at constant pressure and $p_0 = 1000$ hPa. The overbar denotes the running horizontal average over a large-scale area.

In (1) and (2), the horizontal wind components, potential temperature, and mixing ratio are directly obtained from the ERA products. However, for accuracy of Q_1 and Q_2 , ω is recomputed following the method described in Tung *et al.* (1999) and Tung and Yanai (2002). The 6-hourly estimates of Q_1 and Q_2 are averaged into daily mean values for the composite study, and are multiplied by a constant, c_p^{-1} , in order to express them in units of equivalent warming/cooling rate (K day^{-1}).

Q_1 and Q_2 can be written as:

$$Q_1 = Q_R + L(\bar{c} - \bar{e}) - \nabla \cdot \overline{s'\mathbf{v}'} - \frac{\partial \overline{s'\omega'}}{\partial p} \quad (3)$$

and

$$Q_2 = L(\bar{c} - \bar{e}) + L\nabla \cdot \overline{q'\mathbf{v}'} + L \frac{\partial \overline{q'\omega'}}{\partial p}, \quad (4)$$

where Q_R is radiative heating rate, c and e are condensation and evaporation respectively per unit mass of air, s is the dry static energy and the prime denotes the deviation from the running average. Equation (3) represents the total effect of radiative heating, latent heat released by net condensation and the horizontal and vertical convergence of fluxes of sensible heat due to subgrid-scale eddies, such as cumulus convection and turbulence. Equation (4), on the other hand, represents the total effect of net condensation and divergence of eddy moisture fluxes due to subgrid-scale eddies. It is customary to ignore the contribution of the eddy horizontal transport terms (third term in Eq. (3) and second term in Eq. (4)) in convection–large-scale interaction (e.g. Yanai and Johnson 1993).

(b) Definition of the onset

Traditionally, the onset of the Australian summer monsoon has been defined using records at Darwin (12°S , 130°E) or stations in its vicinity (e.g. Troup 1961; Nicholls *et al.* 1982; Hendon and Liebmann 1990a). In the present study, in order to capture the large-scale circulation changes before and after the onset, low-level (850 hPa) westerly wind and convective activity (OLR, precipitation) over a region including northern Australia and the Arafura Sea ($2\text{--}15^\circ\text{S}$, $115\text{--}150^\circ\text{E}$; hereafter NAU; see Fig. 1) are used to determine the onset dates.

The first day with average 850 hPa zonal wind exceeding 2 m s^{-1} over NAU is chosen as the onset day when the westerly wind is sustained for longer than 10 days and the OLR is lower than 210 W m^{-2} for at least several days during the 10-day period. Figure 2 shows an example of mean zonal winds for NAU in the 1979–80 Australian summer monsoon season. The monsoon westerlies abruptly increased in a layer below

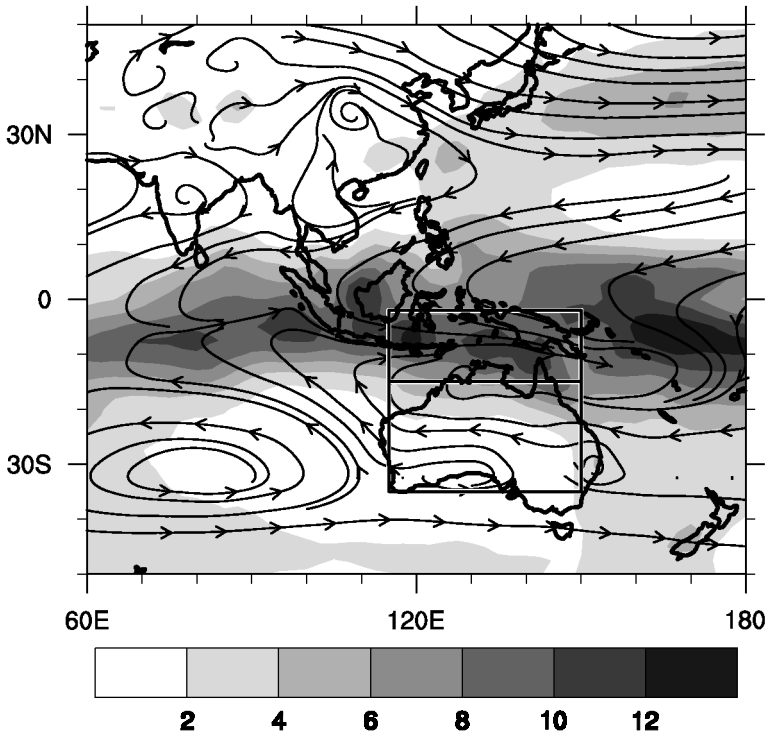


Figure 1. European Centre for Medium-Range Weather Forecasts reanalysis 850 hPa streamlines and precipitation rate (mm day^{-1}) from the Climate Prediction Center Merged Analysis of Precipitation, averaged over December-February 1979-93. The northern and southern rectangular boxes show the northern Australia-Arafura Sea (NAU) and Australian continent (AUC) regions, respectively.

500 hPa during late December-early January over NAU (Fig. 2(a)). These low-level westerlies appeared with strong upper-level easterlies. The value of average 850 hPa zonal wind (Fig. 2(b)) along with the OLR data (not shown) then defined the onset date as 28 December for this case. In this example, two monsoon active periods can be recognized in December-February, and a break (850 hPa zonal wind lower than 2 m s^{-1}) is observed for 16-24 January.

Based on the same definition, the onset dates for monsoon seasons in 1979-93 were chosen and are listed in Table 1. The onset dates selected by the present study are close to previous results. The 14-event mean onset date is 25 December, which is the same as the result by Hendon and Liebmann (1990a) for 30 years (1957-87). The standard deviation of the onset date obtained in the present study is 14 days, which is close to previous results (16 days by Hendon and Liebmann 1990a; 15 days by Holland 1986).

The 14-event composites of all variables were made relative to the onset dates. 'Day 0' denotes the onset day, and positive (negative) values of dates represent days after (before) the onset. Figure 3 is an example showing the composite of zonal wind component. It is clearly seen in NAU that the lower level westerlies abruptly increased after day 0 (Fig. 3(a)), because we define the onset day mainly based on the 850 hPa zonal wind. However, the composite does show some other interesting features. The lower-level westerlies appear with upper-level easterlies, which are strongest at 100 hPa. The first monsoon active period lasts about 30 days. After a monsoon break of

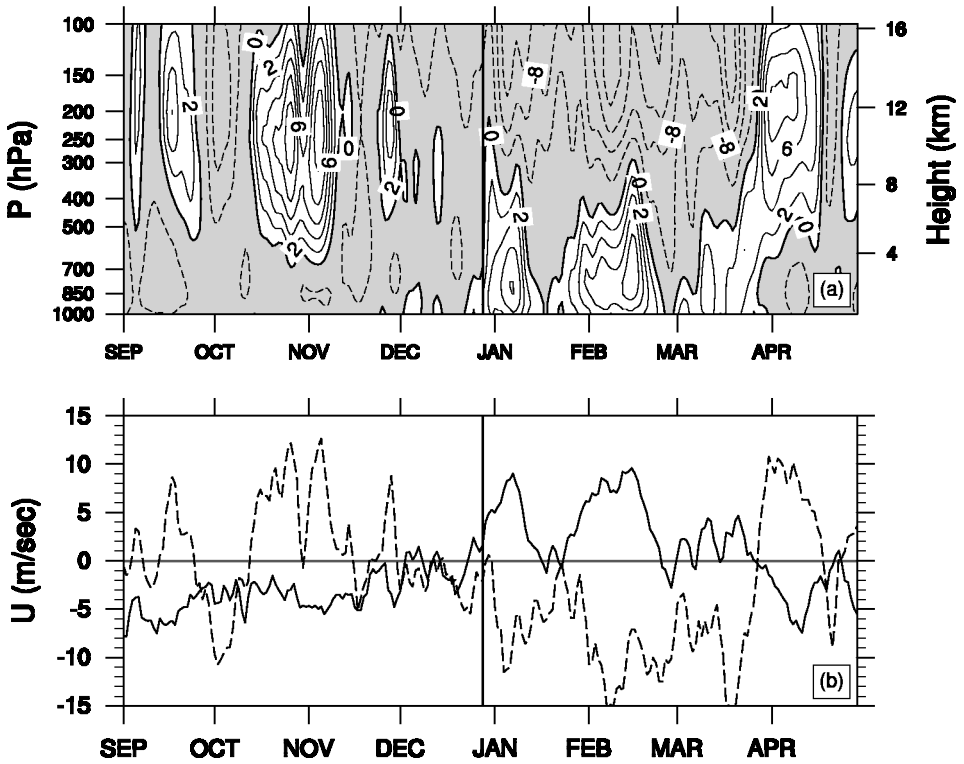


Figure 2. (a) Time-height section of zonal wind speed (contour interval 2 m s^{-1} for positive and 4 m s^{-1} for shaded negative values) and (b) time series of zonal wind speed at 850 hPa (solid line) and 200 hPa (dashed line) in the northern Australia–Arafura Sea region from September 1979 to April 1980. The line at 28 December indicates the monsoon onset day in this case.

TABLE 1. ONSET DATES OF THE AUSTRALIAN SUMMER MONSOON OBTAINED IN THIS STUDY, AND FROM HENDON AND LIEBMANN (1990a)

Season	Dates from this study	Dates from Hendon and Liebmann
1979–80	28 December	29 December
1980–81	4 January	4 January
1981–82	27 November	23 November
1982–83	31 December	7 January
1983–84	5 January	5 January
1984–85	8 December	10 December
1985–86	14 January	16 January
1986–87	13 January	14 January
1987–88	14 December	
1988–89	9 December	
1989–90	6 January	
1990–91	20 December	
1991–92	31 December	
1992–93	17 December	

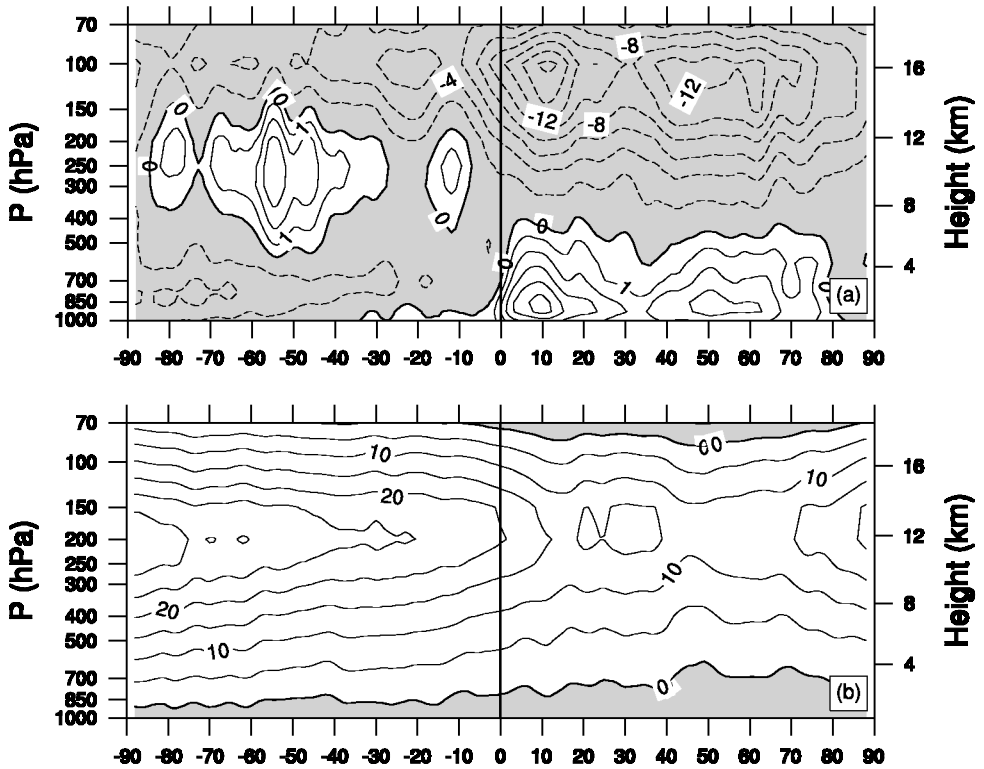


Figure 3. Time-height composites (1979–93) of zonal wind speed over (a) northern Australia–Arafura Sea region (contour interval 1 m s^{-1} for positive and 2 m s^{-1} for negative values) and (b) Australian continent region (contour interval 5 m s^{-1}), relative to the monsoon onset day. Positive (negative) dates represent days after (before) the onset. Negative values are shaded.

about 6 days, the second active monsoon period starts and remains slightly longer than the first one. This is the composite result, so it shows only the general features and does not mean that every year has the same active and break periods. However, the standard error of zonal wind at all levels below 500 hPa is only about 1 m s^{-1} , and, of the 14 monsoon cases, 11 have two monsoon active periods within 90 days from the onset day. Thus, we may conclude that there are about two active periods in a typical monsoon season.

In order to compare the atmospheric structure over NAU and over Australia, we define another region, the Australian continent (AUC), along the same longitudinal boundaries as NAU, but shifted poleward to cover the whole continent ($15\text{--}35^\circ\text{S}$, $115\text{--}150^\circ\text{E}$; see Fig. 1). The composite zonal wind field over the AUC shows that the westerly jet is at the level of about 200 hPa (Fig. 3(b)). It moves poleward to a place outside the AUC as the season progresses from spring to summer, so the averaged zonal wind over the AUC gets weak before the onset. The poleward movement of the jet was documented in an early study by Radok and Grant (1957).

3. COMPOSITE FEATURES OF HEAT SOURCES AND MOISTURE SINKS

It is well known that the Tibetan plateau acts as an elevated heat source in the northern hemisphere spring–summer (e.g. Yanai *et al.* 1992). The heating leads to

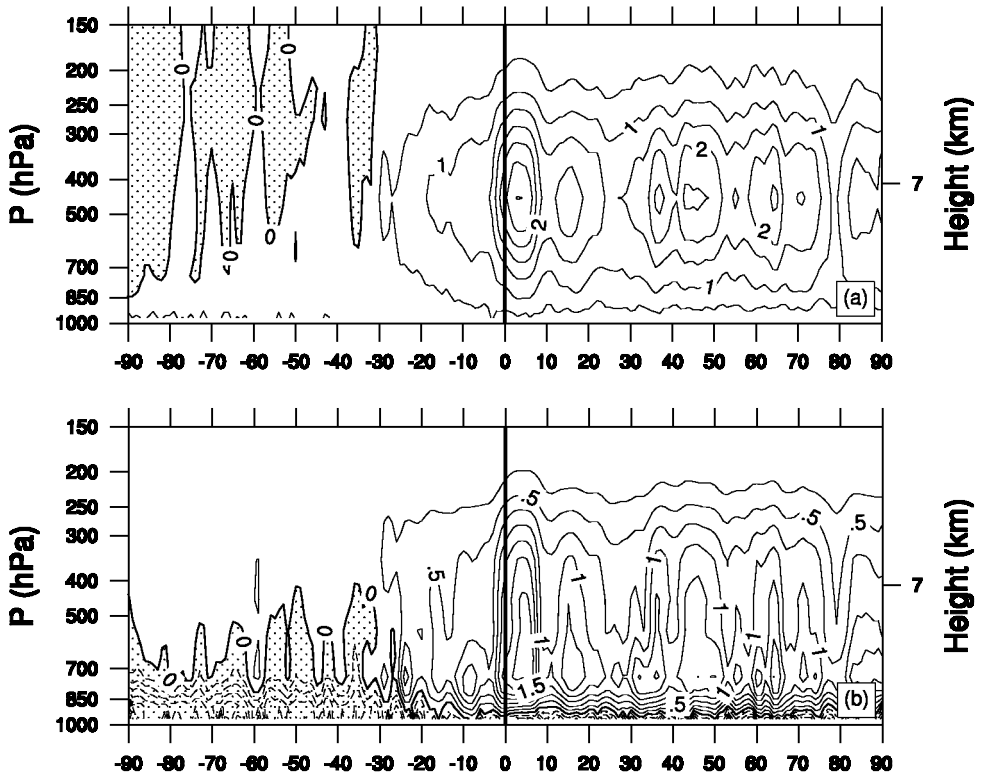


Figure 4. Time–height composites (1979–93) of (a) apparent heat source (contour interval 0.5 K day^{-1}) and (b) apparent moisture sink (contour interval 0.25 K day^{-1}) for northern Australia–Arafura Sea region. Positive (negative) dates represent days after (before) the monsoon onset. Negative values are shaded.

a reversal of the meridional temperature gradient south of the plateau in the upper troposphere (500–200 hPa), and the onset of the Asian summer monsoon is concurrent with it (e.g. Flohn 1957; Li and Yanai 1996). In contrast, the upper troposphere does not exhibit similar structure in the southern hemisphere spring–summer in the Australian summer monsoon region. The Australian continent does not have such high land to produce large-scale elevated heating, and the sensible heating over the AUC is observed only at the lower level (below 750 hPa).

The vertical distributions of heating over Australia have been examined by previous studies. Using data from the Wangara experiment (15 July–27 August 1967; Clarke *et al.* 1971), surface heat flux over the southeastern Australian continent has been studied (e.g. Yamada and Mellor 1975). Schaack *et al.* (1990) used the ECMWF Global Weather Experiment data from December 1978 to November 1979 to calculate the 3-dimensional heating rate through a vertical integration of the isentropic mass continuity equation. They found that the maximum Q_1 over northern Australia in January is about 2.3 K day^{-1} and its peak is located between 500 and 400 hPa. With their method, however, Q_2 is not obtainable. Frank and McBride (1989) used the data obtained from the AMEX (13 January–14 February 1987) rawinsonde network to calculate the heat and moisture budgets at 6-hour intervals. The network is located in the Gulf of Carpentaria, so the results mostly represent the vertical heating distribution over northern Australia.

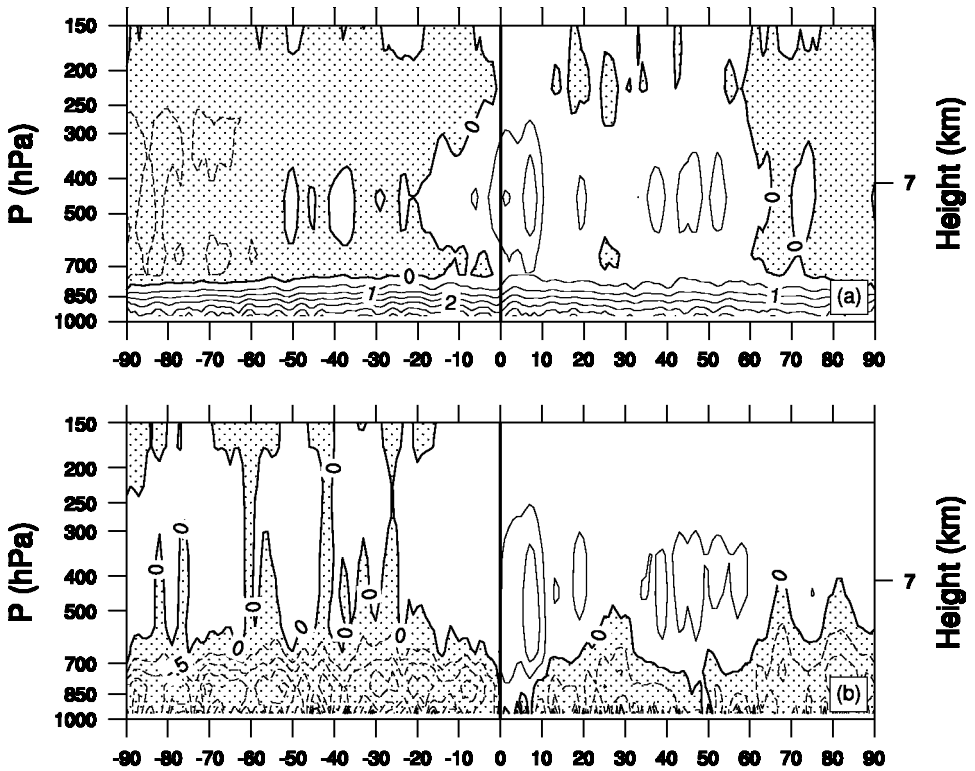


Figure 5. As Fig. 4, but for the Australian continent region.

Our results provide a more general heating structure by making composites from data over the period 1979–93. The vertical profile of Q_1 over NAU shows the maximum heating between 500 and 400 hPa after the onset, although there is relatively weak heating prior to the onset in roughly the same layer (Fig. 4(a)). The maximum does not move in the vertical after the onset. This agrees with Frank and McBride's (1989) finding that the maximum Q_1 does not change much in height during different stages of convective systems.

After the onset, the vertical Q_2 profile over NAU (Fig. 4(b)) has a peak between 800 and 650 hPa, which is lower in height than the peak of Q_1 . This suggests contributions from eddy vertical transports due to deep cumulus convection in the Australian summer monsoon region. The well-separated Q_1 and Q_2 peaks in the vertical are typical features of a deep convective atmosphere (Yanai *et al.* 1973). Besides this lower Q_2 maximum, the distribution exhibits a second peak of Q_2 in a layer between 500 and 400 hPa in some periods. This second peak is located at about the same pressure level as the Q_1 peak. It indicates the presence of rain from stratiform cloud in NAU during the monsoon season.

In contrast, the vertical distribution of Q_1 over the AUC has a very different structure. Significant heating is confined to a shallow layer (surface to 750 hPa) (Fig. 5(a)). Over the AUC, Q_2 (Fig. 5(b)) is negative (about -0.5 K day^{-1}) below 700 hPa. The negative Q_2 value implies moistening due to net evaporation near the surface. All the values of Q_1 below 750 hPa ($\sim 2.5 \text{ K day}^{-1}$) before and after onset are larger than Q_2 , and the maximum Q_1 is near the surface. With the evidence of a warm surface (e.g. Yamada

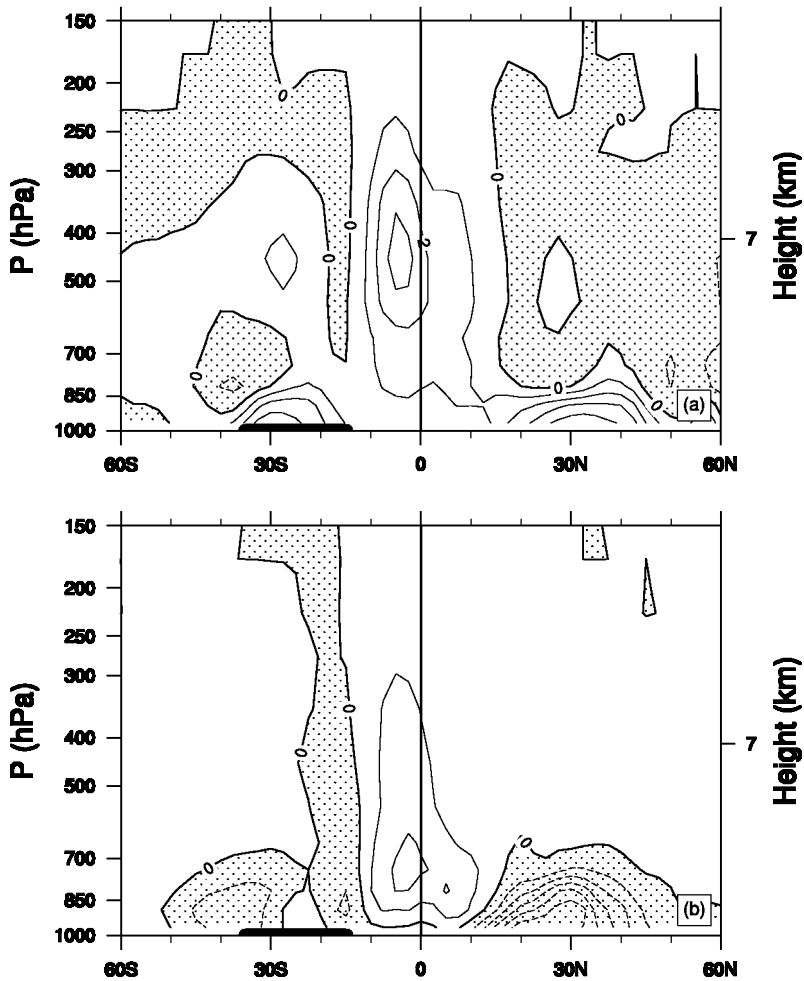


Figure 6. Latitude–height composites (1979–93) of (a) apparent heat source and (b) apparent moisture sink (contour interval 1 K day^{-1}), averaged over $115\text{--}150^\circ\text{E}$ from 7 days to 1 day before the monsoon onset. Negative values are shaded.

and Mellor 1975), it is concluded that the strong heating observed in the shallow layer is caused by sensible heat flux from the ground surface. Actually, the sensible heating in a layer below 750 hPa over the Australian continent starts in September prior to the monsoon onset, so the sensible heating is constantly observed from the composite result over the period shown in Fig. 5(a).

In order to get a clearer view of the heating structure, the meridional–vertical distributions of Q_1 and Q_2 profiles for pre-onset (days -7 to -1) and post-onset (days 0 to 6) periods are averaged over the Australian sector and shown in Figs. 6 and 7. The heating over the Australian continent is constantly observed below 750 hPa in both periods, but the location of deep convection near the equator shows a sudden poleward shift after the onset. This deep convective heating centred at 5°S in the pre-onset period (Fig. 6) is associated with the migrating intertropical convergence zone (ITCZ). It suddenly jumps poleward $5\text{--}10$ degrees and covers a larger region after the onset (Fig. 7). The maximum of Q_1 in the ITCZ is always at 500–400 hPa, but the

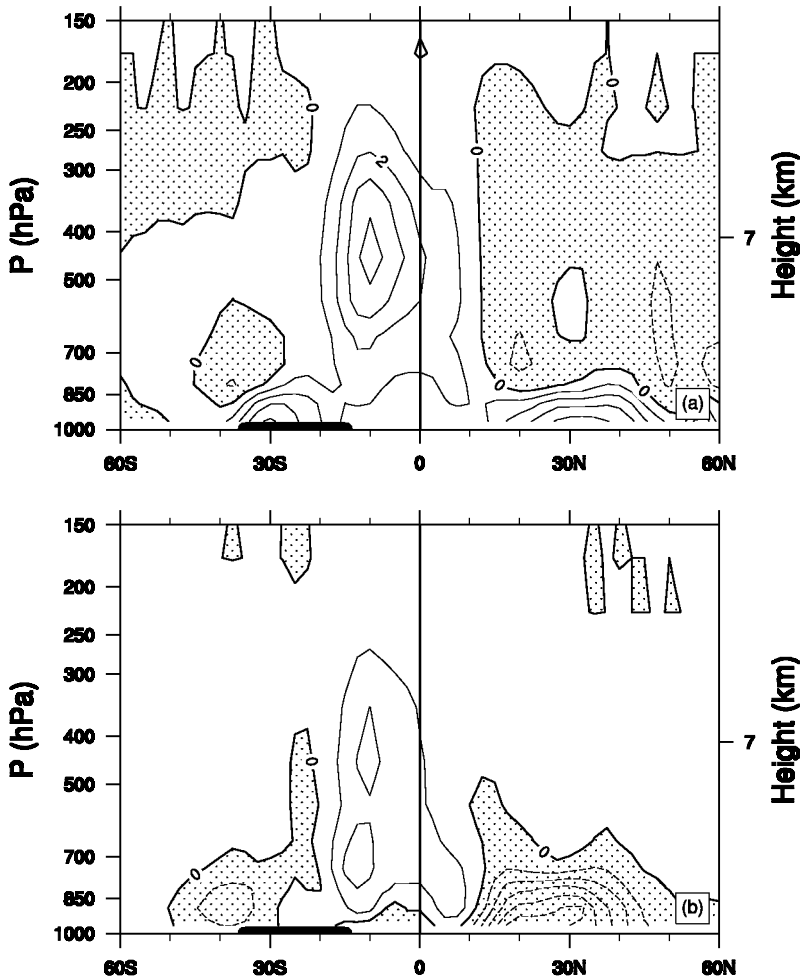


Figure 7. As Fig. 6, but averaged from the onset day to 6 days later.

profile of Q_2 with one lower peak changes to double peaks at 800–650 hPa and 500–400 hPa after the onset. The vertical profiles of Q_1 and Q_2 after the onset are similar to the major mode found by Tung *et al.* (1999) during the Tropical Ocean–Global Atmosphere (TOGA) Coupled Ocean–Atmosphere Response Experiment (COARE) Intensive Observing Period (IOP). These profiles indicate that this structure is a typical mode during the convective phase of the MJO.

4. FACTORS CONTRIBUTING TO THE ONSET

(a) Land–sea thermal contrast

With the contribution of the sensible heating from the surface, a reversal of meridional temperature gradient between the Australian continent and the Arafura Sea in a layer below 800 hPa occurs from September to March. The composite 1000 hPa temperature (Fig. 8) shows a band of very warm air caused by surface heating at 15–30°S in the Australian sector. Before the monsoon onset, the maximum temperature over the

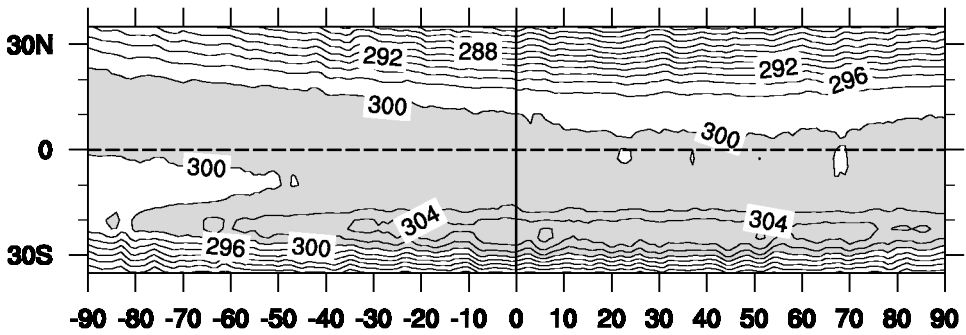


Figure 8. Time-latitude composites (1979–93) of 1000 hPa temperature (K) averaged over 115–150°E. Values greater than 300 K are shaded.

continent exceeds 304 K, which is about 2 to 4 K higher than the air temperature over the ocean near the equator. This warming starts from two to three months prior to the onset. It makes the meridional temperature gradient negative between land and sea, because the air temperature over the Arafura Sea shows only a very small change.

The latitude–height distribution of temperature along the Australian sector indicates that such reversal of the meridional temperature gradient exists from the surface to about 800 hPa before the onset (Fig. 9(a)). The distribution of relative humidity (RH) (Fig. 9(b)) shows that the air over the continent is dry (RH \sim 40–50%), and the moist air (RH \sim 80%) is confined to the equatorial region.

The sensible heating over Australia sets up a thermally induced meridional–vertical circulation, as seen from the outflow above 700 hPa and low-level inflow below 925 hPa over the continent (Fig. 10(a)). Originally, this meridional–vertical circulation is a separate system from the circulation associated with the ITCZ near the equator. The low-level inflow transports moist air inland and intensifies the monsoon circulation in NAU. A narrow region of downward motion near 15°S, between the ascending branch of the ITCZ and the upward motion induced by sensible heating, can be clearly seen in Fig. 10(a). However, these two regions with upward motion merge together, and the narrow area with downward motion disappears after the onset of the monsoon (Fig. 10(b)). Plumb and Hou (1992) discussed the role of subtropical heating in inducing the meridional circulation in an idealized zonally symmetric model. Kawamura *et al.* (2003) suggested the importance of the thermal heat low in creating a convectively unstable condition for the onset of the Australian summer monsoon.

(b) Barotropic instability

Several authors applied dynamic instability theories to the monsoon onset (e.g. *inertial instability* (Tomas and Webster 1997) and *moist baroclinic instability* (Moorthi and Arakawa 1985; Xie and Saiki 1999)). Over the Australian sector, the monsoon westerlies occur north of 15°S, where the atmosphere is nearly barotropic (see Fig. 9(a)). Here, we examine the possible role of barotropic instability in the onset of the Australian summer monsoon. The stability of the barotropic zonal current was discussed by Kuo (1949) for the westerly zonal current and by Nitta and Yanai (1969) for the easterly basic flow. The changing sign of the meridional gradient of the absolute vorticity is a necessary condition for barotropic instability in zonal currents.

In order to see the relevance of barotropic instability to the onset of the Australian monsoon, we calculate the meridional gradients of absolute vorticity at 850 hPa in a

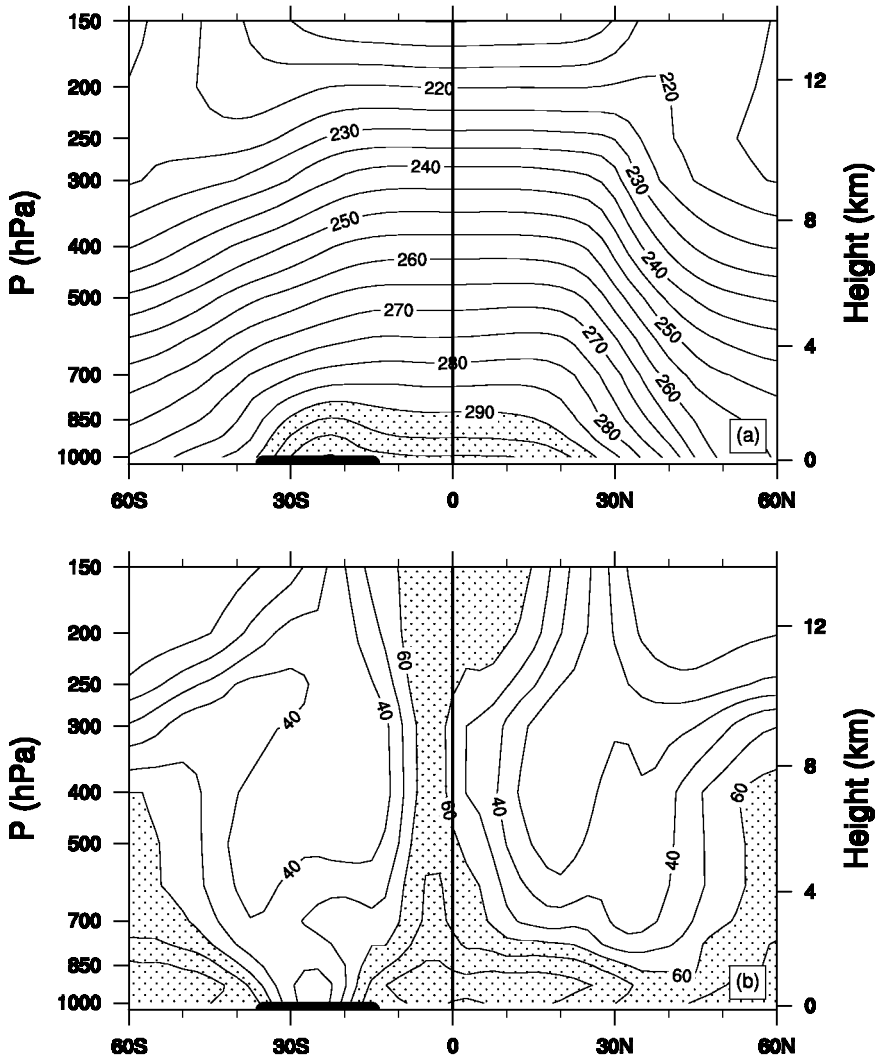


Figure 9. As Fig. 6, but for (a) temperature (K) (values greater than 290 K are shaded) and (b) relative humidity (%) (values greater than 60 are shaded).

zone ($10\text{--}15^{\circ}\text{S}$) where the monsoon westerlies usually occur and negative meridional gradients appear before the onset. The 850 hPa level is chosen because the zonal wind there is used to define the monsoon onset in section 2. Figure 11(a) shows the meridional gradients in this zone averaged over $115\text{--}150^{\circ}\text{E}$ in time–latitude sections from 19 November to 18 January of each year. Nine of the total fourteen cases in 1979–93 show negative meridional gradients of absolute vorticity at least 3 days before the monsoon onset. Five exceptional cases are the monsoon seasons in 1979–80, 1982–83, 1988–89, 1990–91 and 1991–92. In 1982–83 and 1991–92, the Australian summer monsoon is very weak due to El Niño. In 1988–89 (a La Niña year), an unusual deep trough from the subtropical region is involved for the onset that occurred outside the $10\text{--}15^{\circ}\text{S}$ zone. In 1979–80 and 1990–91, the onsets took place in the western and eastern parts of the NAU region, respectively, so the onset area is not centred in the Australian sector.

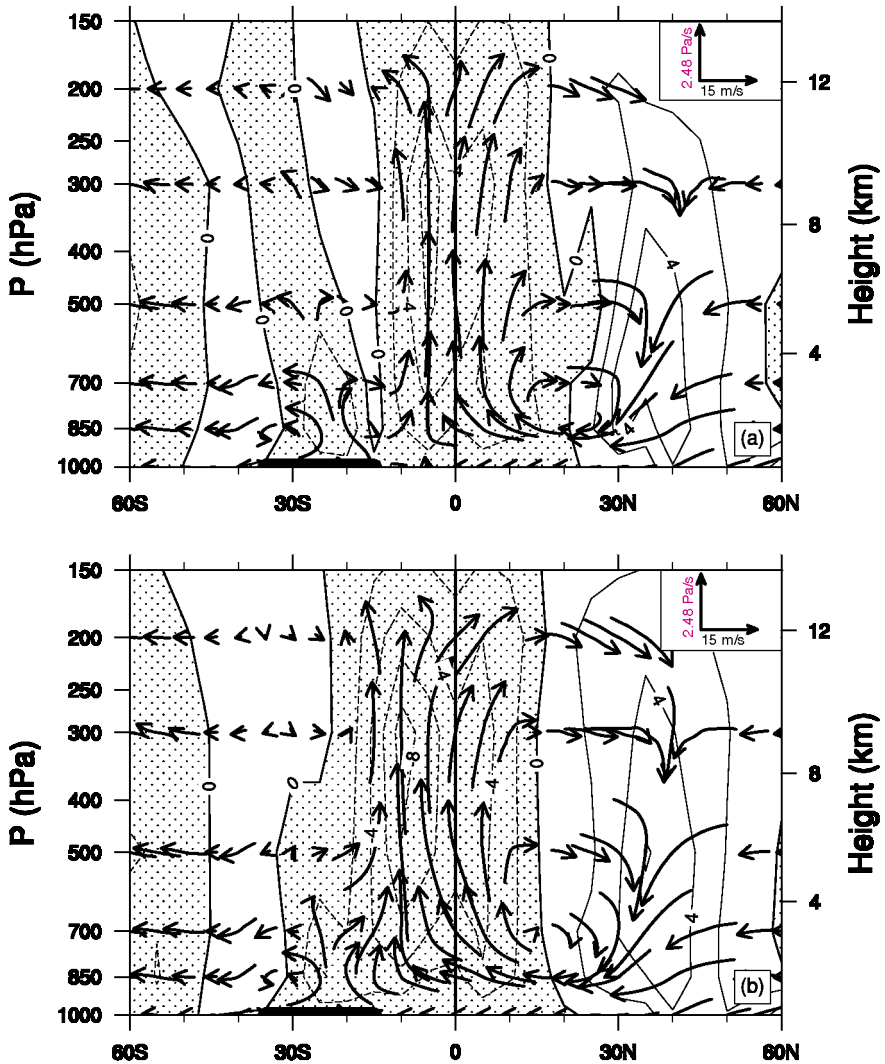


Figure 10. Latitude-height composites (1979–93) of the meridional circulation (arrows) and vertical velocity (contour interval 2 Pa s^{-1}) averaged over $115\text{--}150^\circ\text{E}$, averaged (a) from 7 days to 1 day before the monsoon onset and (b) from the onset day to 6 days later. Areas of ascent (negative ω) are shaded.

A 14-event composite of the mean meridional gradients of absolute vorticity was made relative to the onset dates to obtain an overall view of the role of the barotropic instability (Fig. 11(b)). This composite time–latitude distribution shows that the negative gradient in the $10\text{--}15^\circ\text{S}$ zone appears 7 days before the onset and disappears after the onset. The horizontal distribution of the meridional gradient of absolute vorticity averaged from 6 days to 1 day before the onset (Fig. 12(a)) shows a negative centre in NAU. This centre ($130\text{--}150^\circ\text{E}$) moves to northeastern Australia and does not remain in NAU after the onset (Fig. 12(b)). These results show that the barotropic instability criterion is often met prior to the onset, and provides a condition favourable for the monsoon to occur.

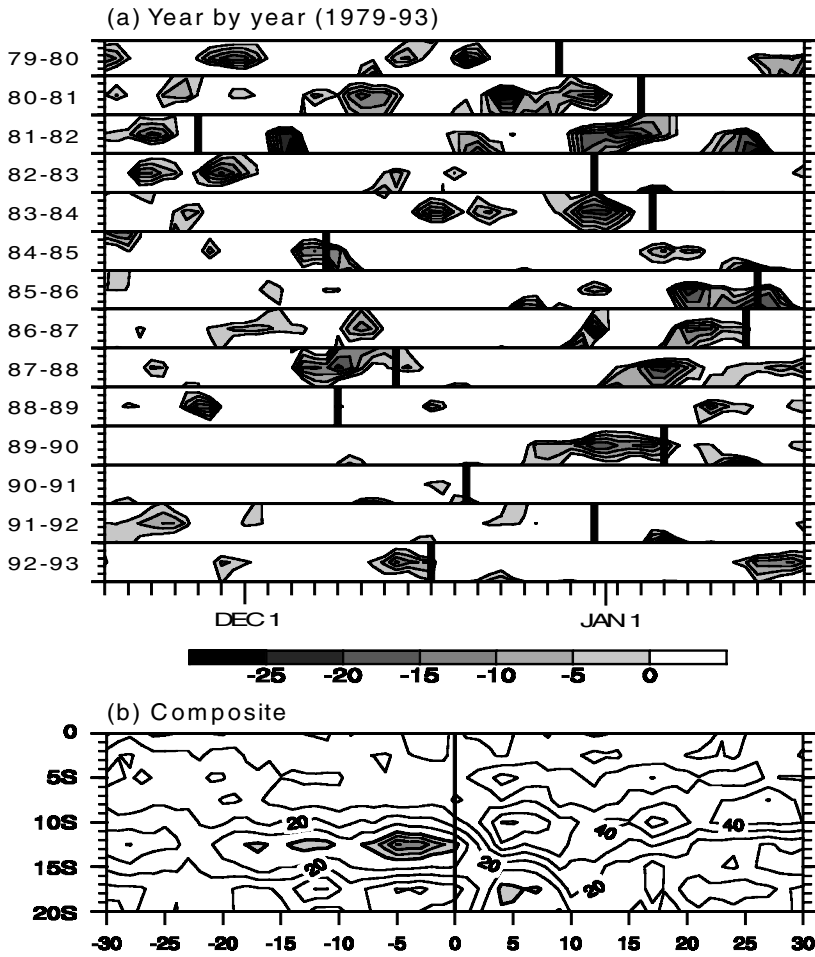


Figure 11. (a) Time–latitude sections of the meridional gradient of absolute vorticity (contour interval $5 \times 10^{-12} \text{ m}^{-1} \text{ s}^{-1}$) at 850 hPa averaged over $115\text{--}150^\circ \text{E}$ (only negative values are shown). The zones between 10°S and 15°S are shown from 19 November to 18 January for each season from 1979/80 to 1992/93. The thick lines indicate the onset days. (b) Time–latitude composite (1979–93) of the meridional gradient of 850 hPa absolute vorticity for 30 days before and after the monsoon onset. The contour interval is $10 \times 10^{-12} \text{ m}^{-1} \text{ s}^{-1}$, and negative values are shaded.

(c) *The arrival of the MJO*

Hendon and Liebmann (1990a,b) suggested, based on a composite study, that the MJO is the major trigger for the Australian summer monsoon onset. They found that the onset coincides with the arrival of the eastward-propagating MJO, which can be traced back to the Indian Ocean for several days.

The time–longitude section of the OLR composite shows the eastward propagation of two MJO events (Fig. 13(a)). The deep convection associated with the first MJO event suddenly intensifies in the Australian sector, and it can be traced back to the Indian Ocean for about 10 days prior to the onset. The land–sea thermal contrast clearly plays an important role in intensifying the vertical circulation in the NAU sector, so the convection with the MJO system in the Australian sector is stronger than that in the Indian Ocean. Although the deep convection associated with the MJO continues to

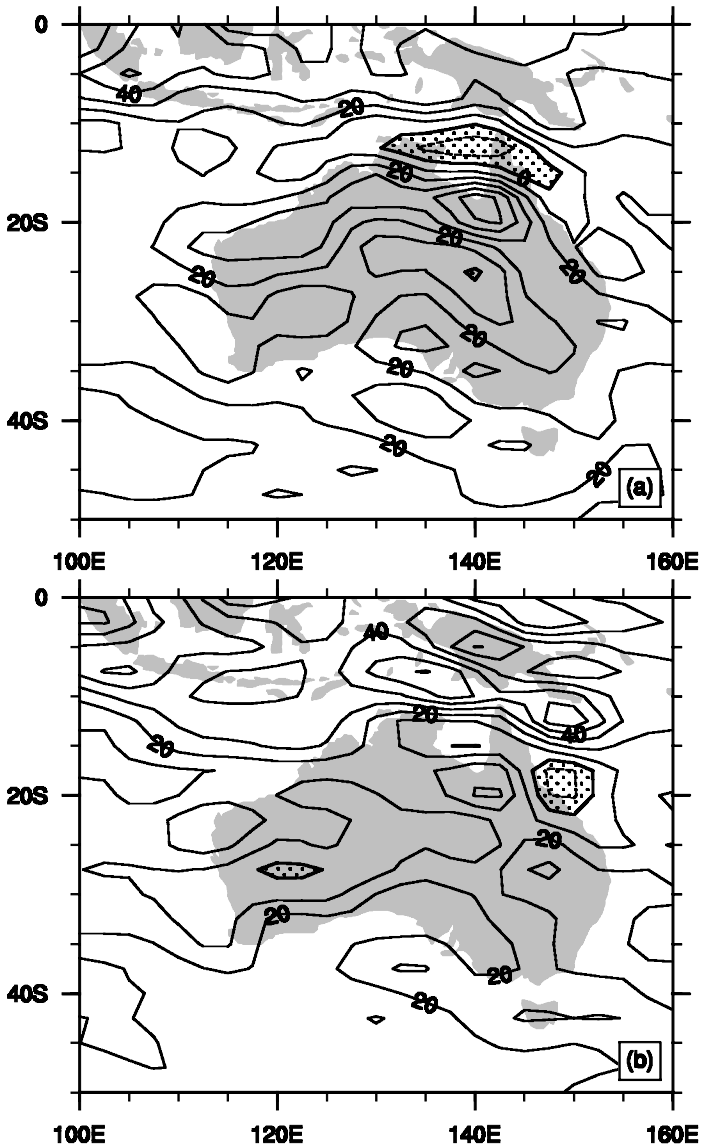


Figure 12. Longitude–latitude composites (1979–93) of the meridional gradient of absolute vorticity (contour interval $10 \times 10^{-12} \text{ m}^{-1} \text{ s}^{-1}$) at 850 hPa, averaged (a) from 7 days before the monsoon onset and (b) from the onset day to 6 days later. Negative values are shaded.

move eastward to the date line, the monsoon system remains in the Australian sector until the monsoon break. The second MJO event after the break can also be traced back to the Indian Ocean.

The time–longitude section of the 850 hPa zonal wind component (Fig. 13(b)) shows an eastward-propagating feature similar to that for OLR, but the centre of active convection observed from OLR leads the westerly wind bursts for several days. However, the maximum upward velocity (not shown) in the 500–400 hPa layer coincides with the centre of deep convection. Yanai *et al.* (2000) provided a detailed case study of

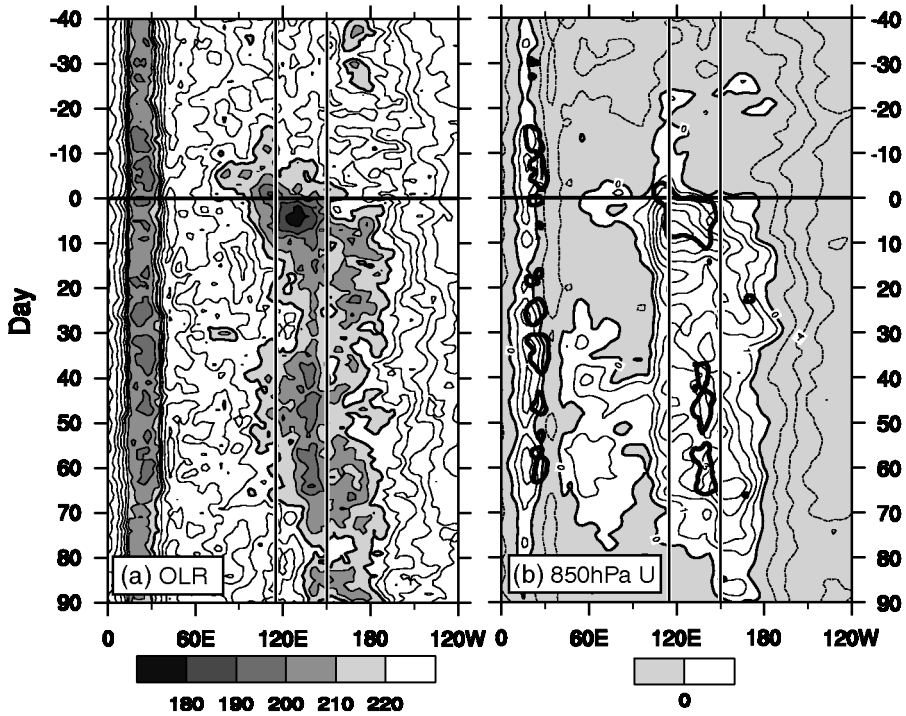


Figure 13. Longitude–time composites (1979–93) of (a) outgoing long-wave radiation (OLR) (contour interval 10 W m^{-2} ; values lower than 220 W m^{-2} are shaded) and (b) 850 hPa zonal wind speed (contour interval 1 m s^{-1} for positive and 2 m s^{-1} for negative values). The thickest lines indicate the 200 W m^{-2} contours of OLR.

MJOs during the TOGA COARE IOP, especially for the phase difference between the zonal wind oscillation and convection.

(d) *The intrusion of the midlatitude trough*

Although the arrival of the MJO is usually concurrent with the onset of the Australian summer monsoon, some years (1981–82, 1988–89, 1990–91) show other disturbances acting as triggers for the onset. For example, in 1990–91, a tropical cyclone located at $5\text{--}20^\circ\text{S}$ moved from 170°E to 150°E during the week before the monsoon onset. It triggered the onset in the eastern part of NAU, resulting in an unusual onset situation. In the 1981–82 and 1988–89 monsoon seasons, the propagation of the MJO was slowed down when it reached the Australian region. An unusually deep trough extending from midlatitudes was observed before the onset in both cases. Davidson *et al.* (1983) have emphasized that midlatitude events (troughs and ridges) play a substantial role in the monsoon onset. They showed several typical synoptic sequences, including a trough over the western coast of Australia prior to the onset. We examined the synoptic sequences for the 14 monsoon cases, and found that only one case (1992–93) had no midlatitude trough involved in the onset. For most cases, the MJO was the major trigger, but the midlatitude trough played a secondary role for the onset. However, when the MJO is weak or absent, the midlatitude trough plays the major role.

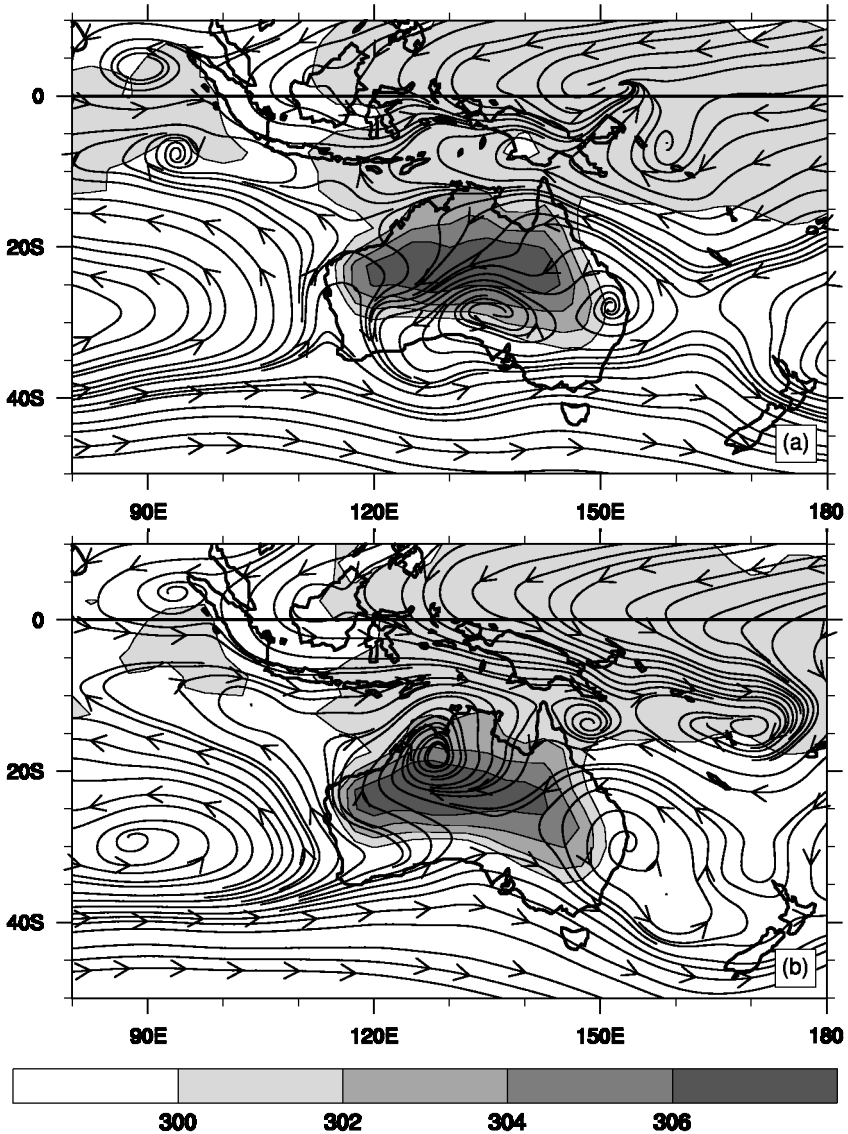


Figure 14. Longitude–latitude composites of 850 hPa streamlines (1979–93): (a) 6 days before the onset and (b) 1 day after the onset. The grey shading is the 1000 hPa temperature (K).

The 14-year composite low-level streamlines and temperature field show the following synoptic sequences. Starting from about one week before the onset, the temperature over the Australian continent increases significantly, while a trough in the mid-latitude westerlies extends to the western coast of Australia (Fig. 14(a)). This trough gradually moves into the continent, and a cyclone is generated in the western part of Australia. When the trough moves further into central Australia, the cyclone merges with the MJO system in NAU. A commonly observed horizontal structure of Australian summer monsoon flow then establishes, as a monsoon low is located in NAU while anticyclones cover the western and eastern sides of Australia (Fig. 14(b)). At this stage, the strong low-level westerlies start and the monsoon onset occurs.

5. CONCLUSIONS

(a) *Heating processes in the Australian region*

In this paper, we have used the ERA data for 1979–93 and Q_1 and Q_2 calculated from heat and moisture budgets to study the onset of the Australian summer monsoon. A 14-event composite relative to the onset dates was used to reveal the onset mechanism. The major findings from the Q_1 and Q_2 diagnosis can be summarized as follows:

(i) Q_1 and Q_2 over northern Australia–Arafura Sea (NAU). The layer of maximum Q_1 is located at 500–400 hPa before and after the onset, but the largest peak of Q_2 after the onset is in a layer between 800 and 650 hPa. The well-separated Q_1 and Q_2 peaks in the vertical imply the presence of deep convection in this area. However, Q_2 has another weaker peak at 500–400 hPa after the onset. This indicates that rain from stratiform cloud is also present.

(ii) Q_1 and Q_2 over the Australian continent (AUC). The maximum Q_1 ($\sim 2.5 \text{ K day}^{-1}$) is confined in a shallow layer near the surface, while Q_2 is negative below 700 hPa. The positive Q_1 suggests sensible heating from the ground surface. This heating starts in September, which is several months before the onset, and contributes to the creation of land–sea thermal contrast in the Australian sector (115–150°E).

(b) *Major factors contributing to the onset*

The four major factors which contribute to the onset of the Australian summer monsoon are summarized as follows:

(i) *Land–sea thermal contrast.* This factor acts as a seasonal preconditioning for the onset. The sensible heating over the Australian continent leads to a reversal of meridional temperature gradient between the Arafura Sea and the Australian continent in a layer below 800 hPa in September–March, and sets up a thermally induced meridional–vertical circulation which helps to transport low-level moist air inland to intensify the monsoon circulation in NAU.

(ii) *Barotropic instability.* Between 15°S and the equator in the Australian sector, the atmosphere is nearly barotropic before the onset. We examined the condition of barotropic instability at 850 hPa where the zonal wind is used to define the monsoon onset. A region of negative meridional gradient of absolute vorticity often appears in NAU prior to the onset and disappears after the onset. This suggests that the barotropic instability is an additional precondition for the monsoon onset.

(iii) *The arrival of the MJO.* The onset of the Australian summer monsoon coincides with the arrival of the eastward-propagating MJO for most cases. The deep convection (observed from OLR), 850 hPa westerlies and ascending motion in the middle troposphere (500–400 hPa) associated with MJOs can be traced back to the Indian Ocean about 10 days prior to the onset. The centre of active deep convection (low OLR) coincides with the vertical velocity at 500–400 hPa, but leads the 850 hPa westerlies for several days.

(iv) *The intrusion of a midlatitude trough.* When the MJO is weak or absent, the onset is triggered by the midlatitude trough or other disturbances. In two cases over the period 1979–93, the midlatitude trough plays a major role in the onset, and in only one case was no trough involved in the onset. The composite synoptic sequences suggest that the intrusion of the midlatitude trough into western Australia plays a supplemental role in the onset, but its importance varies case by case.

ACKNOWLEDGEMENTS

The authors thank two anonymous reviewers for their useful comments on the manuscript. The suggestions from A. Hall, J. D. Neelin, M. Raphael, H. Su, S.-P. Weng, and J.-Y. Yu are appreciated. Special thanks are due to W.-W. Tung for her help with the calculations of Q_1 and Q_2 . The computations were performed at the National Center for Atmospheric Research Scientific Computing Division and University of California Los Angeles Department of Atmospheric Sciences. This work was supported by the National Oceanic and Atmospheric Administration under Grant NA96GP0331 and by the National Science Foundation under Grant ATM-9902838.

REFERENCES

- Berson, F. A. 1961 Circulation and energy balance in a tropical monsoon. *Tellus*, **13**, 472–485
- Chao, W. C. 2000 Multiple quasi-equilibria of the ITCZ and the origin of monsoon onset. *J. Atmos. Sci.*, **57**, 641–652
- Chao, W. C. and Chen, B. 2001 On the origin of monsoons. *J. Atmos. Sci.*, **58**, 3497–3507
- Clarke, R. H., Dyer, A. J., Brook, R. R., Reid, D. G. and Troup, A. J. 1971 'The Wangara experiment: Boundary layer data.' Tech. Paper 19, Div. Meteorol. Phys., CSIRO, Melbourne, Australia
- Davidson, N. E., McBride, J. L. and McAvaney, B. J. 1983 The onset of the Australian monsoon during winter MONEX: synoptic aspects. *Mon. Weather Rev.*, **111**, 496–516
- Flohn, H. 1957 Large-scale aspects of the 'summer monsoon' in South and East Asia. *J. Meteorol. Soc. Jpn.*, 75th Ann. Vol., 180–186
- Frank, W. M. and McBride, J. L. 1989 The vertical distribution of heating in AMEX and GATE cloud clusters. *J. Atmos. Sci.*, **46**, 3464–3478
- Gibson, J. K., Källberg, P., Uppala, S., Hernandez, A., Nomura, A. and Serrano, E. 1997 ERA Description, Project Report Series. ERA-15 No. 1. European Centre for Medium-Range Weather Forecasts, Reading, UK
- Hendon, H. H., Davidson, N. E. and Gunn, B. 1989 Australian summer monsoon onset during AMEX 1987. *Mon. Weather Rev.*, **117**, 370–390
- Hendon, H. H. and Liebmann, B. 1990a A composite study of onset of the Australian summer monsoon. *J. Atmos. Sci.*, **47**, 2227–2240
- 1990b The intraseasonal (30–50 day) oscillation of the Australian summer monsoon. *J. Atmos. Sci.*, **47**, 2909–2923
- Holland, G. J. 1986 Interannual variability of the Australian summer monsoon at Darwin; 1952–82. *Mon. Weather Rev.*, **114**, 594–604
- Hunt, H. A., Taylor, G. and Quayle, E. T. 1913 *The climate and weather of Australia*. Government Printer, Melbourne, Australia
- Kawamura, R., Fukuta, Y., Ueda, H., Matsuura, T. and Iizuka, S. 2002 A mechanism of the onset of the Australian summer monsoon. *J. Geophys. Res.*, **107**, D14, doi: 10.1029/2001JD001070
- Kuo, H. L. 1949 Dynamic instability of two-dimensional non-divergent flow in a barotropic atmosphere. *J. Meteorol.*, **6**, 105–122
- Li, C. and Yanai, M. 1996 The onset and interannual variability of the Asian summer monsoon in relation to land–sea thermal contrast. *J. Climate*, **9**, 358–375
- Madden, R. A. and Julian, P. R. 1971 Detection of a 40–50 day oscillation in the zonal wind in the tropical Pacific. *J. Atmos. Sci.*, **28**, 702–708
- 1972 Description of global scale circulation cells in the tropics with 40–50 day period. *J. Atmos. Sci.*, **29**, 1109–1123
- McBride, J. L. 1987 The Australian summer monsoon. Pp. 203–231 in *Reviews of Monsoon Meteorology*. Eds. C. P. Chang and T. N. Krishnamurti. Oxford University Press, Oxford, UK
- Manton, M. J. and McBride, J. L. 1992 Recent research on the Australian monsoon. *J. Meteorol. Soc. Jpn.*, **70**, 275–285
- Moorthi, S. and Arakawa, A. 1985 Baroclinic instability with cumulus heating. *J. Atmos. Sci.*, **42**, 2007–2031
- Murakami, T. and Sumi, A. 1982a Southern Hemisphere monsoon circulation during the 1978–79 WMONEX. Part I: Monthly mean wind fields. *J. Meteorol. Soc. Jpn.*, **60**, 638–648

- Murakami, T. and Sumi, A. 1982b Southern Hemisphere monsoon circulation during the 1978–79 WMONEX. Part II: Onset, active and break monsoons. *J. Meteorol. Soc. Jpn.*, **60**, 649–671
- Nicholls, N., McBride, J. L. and Ormerod, R. J. 1982 On predicting the onset of the Australian wet season at Darwin. *Mon. Weather Rev.*, **110**, 14–17
- Nitta, T. and Yanai, M. 1969 A note on the barotropic instability of the tropical easterly current. *J. Meteorol. Soc. Jpn.*, **47**, 127–130
- Plumb, R. A. and Hou, A. Y. 1992 The response of a zonally symmetric atmosphere to subtropical thermal forcing: Threshold behavior. *J. Atmos. Sci.*, **49**, 1790–1799
- Radok, U. and Grant, A. M. 1957 Variations in the high tropospheric mean flow over Australia and New Zealand. *J. Meteorol.*, **14**, 141–149
- Schaack, T. K., Johnson, D. R. and Wei, M.-Y. 1990 The three-dimensional distribution of atmospheric heating during GWE. *Tellus*, **42A**, 305–327
- Tomas, R. A. and Webster, P. J. 1997 The role of inertial instability in determining the location and strength of near-equatorial convection. *Q. J. R. Meteorol. Soc.*, **123**, 1445–1482
- Troup, A. J. 1961 Variations in upper tropospheric flow associated with the onset of the Australian summer monsoon. *Indian J. Meteorol. Geophys.*, **12**, 217–230
- Tung, W.-W. and Yanai, M. 2002 Convective momentum transport observed during the TOGA COARE IOP. Part I: General features. *J. Atmos. Sci.*, **59**, 1857–1871
- Tung, W.-W., Lin, C., Chen, B., Yanai, M. and Arakawa, A. 1999 Basic modes of cumulus heating and drying observed during TOGA-COARE IOP. *Geophys. Res. Lett.*, **26**, 3117–3120
- Webster, P. J. 1987 The elementary monsoon. Pp. 3–32 in *Monsoons*. Eds. J. S. Fein and P. L. Stephens, John Wiley, New York
- Webster, P. J., Magana, V. O., Palmer, T. N., Shukla, J., Tomas, R. A., Yanai, M. and Yasunari, T. 1998 Monsoons: Processes, predictability, and the prospects for prediction. *J. Geophys. Res.*, **103**, 14451–14510
- Xie, P. P. and Arkin, P. A. 1997 Global precipitation: A 17-year monthly analysis based on gauge observations, satellite estimates, and numerical model outputs. *Bull. Am. Meteorol. Soc.*, **78**, 2539–2558
- Xie, S.-P. and Saiki, N. 1999 Abrupt onset and slow seasonal evolution of summer monsoon in an idealized GCM simulation. *J. Meteorol. Soc. Jpn.*, **77**, 949–968
- Yamada, T. and Mellor, G. 1975 A simulation of the Wangara atmospheric boundary layer data. *J. Atmos. Sci.*, **32**, 2309–2329
- Yanai, M. and Johnson, R. H. 1993 Impacts of cumulus convection on thermodynamic fields. Pp. 39–62 in *The Representation of Cumulus Convection in Numerical Models of the Atmosphere*, Meteorol. Monograph, No. 46, American Meteorological Society, Boston, USA
- Yanai, M., Esbensen, S. and Chu, J. H. 1973 Determination of bulk properties of tropical cloud clusters from large-scale heat and moisture budgets. *J. Atmos. Sci.*, **30**, 611–627
- Yanai, M., Li, C. and Song, Z. 1992 Seasonal heating of the Tibetan Plateau and its effects on the evolution of the Asian summer monsoon. *J. Meteorol. Soc. Jpn.*, **70**, 319–351
- Yanai, M., Chen, B. and Tung, W.-W. 2000 The Madden-Julian oscillation observed during the TOGA COARE IOP; Global view. *J. Atmos. Sci.*, **57**, 2374–2396